31st Annual International Conference of the IEEE EMBS
Minneapolis, Minnesota, USA, September 2-6, 2009

Complete Angle Small Animal Fluorescence Imaging with Early-Arriving Photons

Mark Niedre and Vasilis Ntziachristos

***Abstract*—Fluorescence mediated tomography allows quantitative, three-dimensional imaging of optical reporter probes in whole animals and is therefore emerging as a powerful molecular imaging tool. The achievable image quality in fluorescence tomography is limited by the high-degree of light scatter in biological tissue. Time-gated detection of early-arriving and therefore minimally-scattered photons transmitted through diffusive tissue is one strategy for minimizing the effects of light scatter. In this work, we performed full-angle tomographic imaging of mice implanted with fluorescent tubes using time-gated detection of early- and later-arriving photons. This was achieved using a femtosecond laser and a high-speed, time-gated intensified CCD imager. We demonstrate that the early-transmitted fluorescent photons allow improved visualization of the fluorescence distribution, even when considering individual projections through the animal. High-fidelity image reconstruction using 72 projections in 5-degree steps using early-arriving photons is also demonstrated.**

I. Introduction

In vivo tomographic imaging in small animals has become a powerful tool for visualizing fluorescent molecular reporters that provide contrast against, for example, cell surface receptors, protease activity and gene expression [1, 2]. Fluorescence mediated tomography (FMT) utilizes multiple source and detector projections through the animal combined with accurate models of diffuse light propagation to generate quantitative, three-dimensional distributions of fluorochromes in tissue [3, 4]. Despite significant advances in instrumentation and image reconstruction algorithms in recent years the achievable imaging resolution in small animal tomography - like clinical-scale diffuse optical tomography – is fundamentally limited by the high-degree of light scatter in tissue.

Temporal gating of transmitted light has been proposed as a technique to reduce the effects of light scatter in biological tissue. Conceptually, the earliest-transmitted photons travel preferentially along a more-direct path between the source and detector compared with the bulk of the diffuse photons in the scattering medium. Therefore, temporal gating should allow tomographic imaging with improved fidelity. The concept has been explored previously by our group and others at the mesoscopic [5], small animal [6] and clinical physical scales [7]. We have recently demonstrated the 'early photon tomography' concept both in complex optical phantoms [8], and in small animals, specifically by imaging Lewis Lung Carcinoma bearing mice labeled with a Cathepsin-sensitive fluorescent probe [6].

Herein, we distinguish the terms 'early-arriving' (or 'early-diffuse') photons from the frequently cited term 'ballistic photons', the latter implying that photons have undergone no (or negligible) scattering during transmission through diffusive tissue. As we demonstrate in this work, 'early-diffuse' photons are multiply scattered, but nevertheless undergone relatively fewer scattering events than, for example, the un-gated (*i.e.* continuous wave; CW) case. They therefore propagate with a significantly stronger forward bias that is highly useful for diffuse optical tomographic imaging applications.

In this work, we utilized a simplified quasi *in vivo* animal model – *i.e.* euthanized mice with implanted fluorescent tubes - specifically to observe the improvement obtained by detecting early- versus later-transmitted photons through the animal. Herein, we demonstrate that the early-transmitted

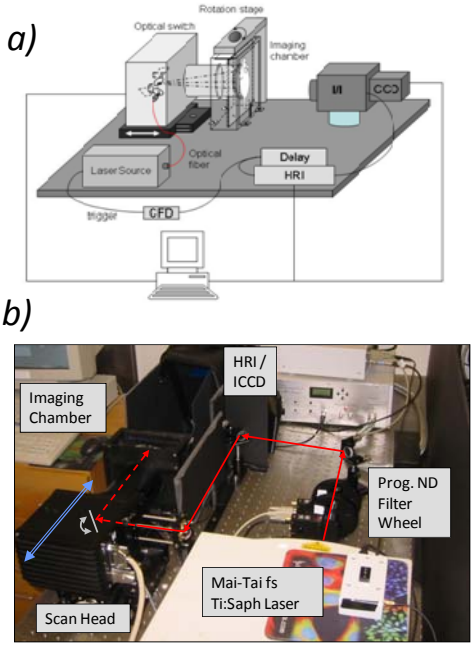

Figure 1. The time-resolved small animal imaging system used in this study. *(a)* schematic of the system with the major components labeled. (I/I = image intensifier, CCD = charge coupled device camera, HRI = high rate imager, CFD = constant fraction discriminator), and *(b)* photograph of the system

Manuscript received October 9, 2001. This research was supported in part by the National Institutes of Health grant R01 EB 000750..

M Niedre is Assistant Professor, Department of Electrical and Computer Engineering, Northeastern University, Boston, MA, 02115, USA, mniedre@ece.neu.edu

V Ntziachristos is Professor and Chair, Institute for Biological and Medical Imaging, Technical University of Munich and Helmholtz Center Munich, Ismaninger str. 21 Munich, Germany, v.ntziachristos@tum.de

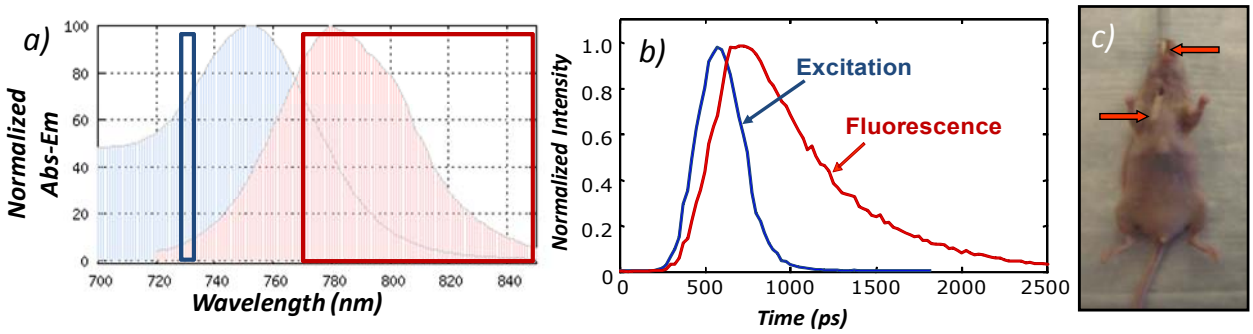

Figure 2 *(a)* absorption (blue) and emission (red) spectra of the Alexafluor-750 dye along with the 'intrinsic' (excitation) and fluorescence detection wavelengths, indicated by overlaid colored rectangles, (b) Typical time-resolved curves transmitted through the imaging chamber, measured at the excitation and emission wavelengths, and *(c)* photograph of mouse with location of fluorescent tubes indicated.

fluorescence photons allow improved visualization of the implanted tubes, even when considering individual projections through the animal. Tomographic reconstructions of the early-arriving fluorescence photon fields are correspondingly shown to be of high fidelity when compared to X-ray CT images of the animal.

II. Methods and Materials.

A. Theory

The diffusion approximation to the Boltzmann Transport Equation (BTE) is frequently used to model photon propagation in diffuse optical tomography applications in the continuous wave (CW), frequency domain (FD) and time-domain (TD) regimes. In an infinite medium, the time-dependent photon fluence rate from a short, pulsed point source at the origin is given by [9]:

$$N(r,t) = \frac{c}{(4\pi Dct)^{3/2}} \exp\left(-\frac{r^2}{4Dct} - \mu_a ct\right) \quad (1)$$

, where D is the diffusion coefficient, μ_a is the absorption coefficient, and c is the speed of light in the medium. At very early times following the light pulse, t, we and others have observed that the time-dependant diffusion equation is not sufficiently accurate for modeling photon propagation and therefore a higher-order approximation to the BTE - for example, the second-order cumulant solution [5] - is required:

$$N(r,t) = \frac{1}{(4\pi D_{zz} ct)^{\frac{1}{2}}} \frac{1}{4\pi D_{xx} ct} exp\left[-\frac{(z - R_z(t))^2}{4D_{zz} ct}\right]$$
$$\ldots \times exp\left[-\frac{(x^2 + y^2)}{4D_{xx} ct}\right] exp(-\mu_a t) \quad (2)$$

, where $R_z(t)$ is the moving center of the photon source, D_{xx} and D_{zz} are the directional diffusion coefficients. In this work, we have experimentally determined that the second-order cumulant approximation accurately models propagation of photons detected at early time gates (defined in detail below).

B. Instrumentation

The system used for the time-resolved measurements is shown in figure 1. A femtosecond laser (MaiTai, Spectra-Physics, Mountain View, California) operating at 732 nm was free-beam coupled into a scanning galvanometer pair. The laser light could be scanned in a non-contact manner across a sample placed in the 2.2 cm wide imaging chamber as desired. The transmitted light was detected with a CCD camera coupled with a gated image intensifier (LaVision Picostar HR12, LaVision GmbH, Goettingen, Germany). A high-rate imager (Kentech Instruments Ltd., Oxfordshire, England) and a picosecond dely unit (Kentech) allowed acquisition of images with minimum gate widths of 200 ps with a temporal step size of 25 ps. The laser power at the sample was approximately 30 mW. Full rotation of the animal was facilitated by a stepper motor driven rotation stage (Newport Corp) with a resolution of 0.01°.

For these experiments, free AlexaFluor-750 (AF750) dye was used as the fluorochrome. A 10 nm bandpass filter centered at 730 nm was used for the intrinsic (excitation) measurements and a long pass filter with a cut-on wavelength of 770 nm was used for measurement of the fluorescence (Chroma Technology Corp). As shown in fig. 2a, this combination of filters allowed the optimal combination of detection of fluorescence light while rejecting contributions of intrinsic light in the fluorescence channel. As shown in fig. 2b, the measured fluorescent full time curve has a significantly longer tail versus the excitation light due to the fluorescence lifetime of the AF750.

C. Animal Experiments

Female nu/nu were euthanized by carbon-dioxide asphyxiation. Plastic, semi-transparent tubes with 1 mm internal diameter were filled with 750 nmol/L AF750 dissolved in intralipid fluid and implanted in the torso of the animal. As shown in fig. 2c, the first tube (1 cm in length) was placed subcutaneously outside the ribcage, and the second (5 cm in length) was inserted in the esophagus, so that the two tubes were approximately parallel, separated by ~7 mm.

D. Data Collection

Mice were inserted into a custom made carbon-fiber tube that supported the upper and lower portions of the animal

body with a 2cm window for optical scanning of the torso. The 2.2 cm imaging chamber was filled with an intralipid solution (μ_s' = 20cm^{-1}, μ_a = 0.3 cm^{-1}) that approximately matched the optical properties of the thoracic cavity of the mouse at 730nm as measured by us previously [10]. The laser was translated across the imaging chamber at 45 beam positions along a line for each projection, and mice were rotated through 360 degrees with 5 degree increments. The ICCD was synchronized to the trigger signal from the laser so as to acquire images at a specific temporal gate. Images were taken at both the intrinsic (excitation) and fluorescence wavelengths. For these experiments, we compared 'early-arriving' and 'later-arriving' photons. The acquisition temporal gate widths and center times (relative to the un-scattered propagation of the pulse through the chamber) for each acquisition were as follows, *i)* early intrinsic: width = 200 ps, center = 200ps, *ii)* early fluorescent: width = 200 ps, center = 300 ps, *iii)* later intrinsic: width = 1000 ps, center = 550 ps, and *iv)* later fluorescent: width = 1000 ps, center = 900 ps. The ICCD could be operated with a maximum gate width of 1000 ps; therefore, the 'later' time gates approximated continuous wave (ungated) photons with our system. ICCD images for each laser source position and rotation angle were segmented into arrays of virtual detectors to generate source-detector projections for each axial slice. The fluorescence data was normalized to the intrinsic data in order to correct for the optical heterogeneity of the animal torso as we have done previously [11].

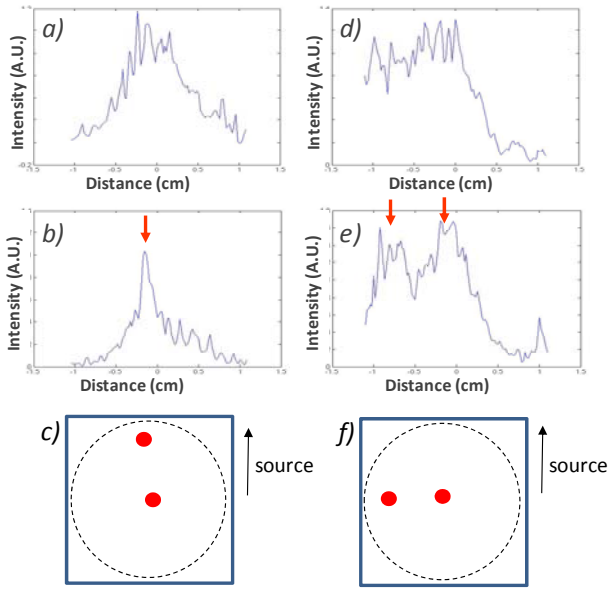

Figure 3. Transmitted fluorescence intensity normalized to the transmitted intrinsic intensity, measured with the ICCD at later *(a,d)* and early*(b,e)* time gates, when the mouse was rotated to 0 degrees *(a-c)* and 90 degrees *(*d-f), respectively. The approximate locations of the fluorescent tubes for each orientation is shown *(c,f)*. With early-photons, separate fluorescent tubes are clearly visible, even when they are located in the center of the 2.2 cm imaging chamber *(d)*.

E. Image Reconstruction

Fluorescence tomographic image reconstructions were performed using our previously reported approach [6]. Briefly, the volume was discretized into 0.5 mm x 0.5 mm x 0.5 mm voxels. Forward modeling of the normalized early-photon density field was calculated using a second-order cumulant approximation to the BTE. Inversion of the matrix equation – relating the source-detector projections to the system sensitivity (weight) functions and unknown fluorochrome concentration - was performed using Singular Value Decomposition (SVD) with Tikhonov regularization.

F. X-Ray Computed Tomography

Following fluorescence imaging, X-ray CT images were acquired on a combined high-resolution single-photon emission CT (SPECT) scanner (Gamma-Medica, X-SPECT, Northridge, CA). Mice were kept in the carbon-fiber tube so that the fluorescence and CT images could be compared. A total of 256 projections were acquired for each mouse, and reconstructions were performed with a filtered back-projection algorithm. Visualizations and 3-D renderings of CT data were performed with the Amira (Mercury-TGS, Chelmsford, MA) and Image-J software packages.

III. RESULTS AND DISCUSSION

Mice with implanted fluorescent tubes were scanned with the imaging system as described above. Figure 3 shows typical normalized fluorescence data at 0 degrees rotation (*i.e.* with the mouse facing the laser so that the tubes were approximately parallel to the z-axis; fig. 3a-c) and at 90 degrees rotation (*i.e.* with the mouse facing sideways so that the tubes were approximately in the center of the chamber perpendicular to the z-axis; fig. 3d-f). With the early-time gate, a significantly narrower transmitted fluorescence profile was visible at 0 degrees relative to the late-time gates. Similarly, when the mouse was oriented at 90 degrees, two distinct fluorescent peaks corresponding to the two tubes were visible, whereas this was effectively 'smeared' at the later time gate, so that two tubes could not be directly distinguished. These projection data demonstrate the advantage of detecting early-photons through small animals, since the fluorescent tubes were significantly easier to visualize even in single projections versus late-arriving photons.

Figure 4 shows the reconstructed early-photon fluorescence image of the two tubes as well as the X-ray CT image at the same axial slice showing the actual location of the tubes. The size, location and separation (7mm) of the tubes in the reconstructed fluorescence image was in excellent agreement with the X-ray CT image.

In summary, we have demonstrated that diffuse fluorescence tomography with early-arriving photons yields very high fidelity image reconstructions. Further, the early-transmitted fluorescence photons allow improved visualization of the implanted fluorescent tubes versus later-

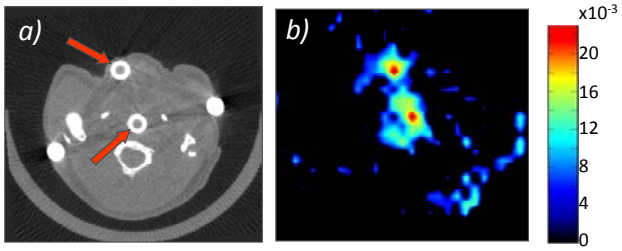

Figure 4. *(a)* Axial X-Ray CT image of the mouse showing the location of the fluorescent tubes, separated by 7 mm, and (b) Reconstructed fluorescence image using early-diffuse photons. The center-to-center separation is 7 mm.

arriving photons, even when considering individual projections through the animal. We further note that the thoracic cavity and in particular the lung region exhibits a very high-degree of optical scatter and attenuation versus other regions of the animals anatomy [10]. As such, an even greater degree of improvement may be observed when imaging other organs with this technique.

ACKNOWLEDGEMENTS

The authors wish to thank Mr. Joshua Dunham for his assistance in animal preparation and Mr. Gregory Wojtkiewicz for acquisition of X-ray CT images..

REFERENCES

[1] Wang, Y., J.Y. Shyy, and S. Chien, *Fluorescence proteins, live-cell imaging, and mechanobiology: seeing is believing.* Annu Rev Biomed Eng, 2008. **10**: p. 1-38.

[2] Giepmans, B.N., et al., *The fluorescent toolbox for assessing protein location and function.* Science, 2006. **312**(5771): p. 217-24.

[3] Ntziachristos, V., et al., *Fluorescence molecular tomography resolves protease activity in vivo.* Nat Med, 2002. **8**(7): p. 757-60.

[4] Hielscher, A.H., *Optical tomographic imaging of small animals.* Curr Opin Biotechnol, 2005. **16**(1): p. 79-88.

[5] Alfano, R.R., et al., *Time-resolved and nonlinear optical imaging for medical applications.* Ann N Y Acad Sci, 1998. **838**: p. 14-28.

[6] Niedre, M.J., et al., *Early photon tomography allows fluorescence detection of lung carcinomas and disease progression in mice in vivo.* Proc Natl Acad Sci U S A, 2008. **105**(49): p. 19126-31.

[7] Wu, J., et al., *Fluorescence tomographic imaging in turbid media using early-arriving photons and Laplace transforms.* Proc Natl Acad Sci U S A, 1997. **94**(16): p. 8783-8.

[8] Turner, G.M., et al., *Complete-angle projection diffuse optical tomography by use of early photons.* Opt Lett, 2005. **30**(4): p. 409-11.

[9] Kienle, A. and M.S. Patterson, *Improved solutions of the steady-state and the time-resolved diffusion equations for reflectance from a semi-infinite turbid medium.* J Opt Soc Am A Opt Image Sci Vis, 1997. **14**(1): p. 246-54.

[10] Niedre, M.J., G.M. Turner, and V. Ntziachristos, *Time-resolved imaging of optical coefficients through murine chest cavities.* J Biomed Opt, 2006. **11**(6): p. 064017.

[11] Soubret, A., J. Ripoll, and V. Ntziachristos, *Accuracy of fluorescent tomography in the presence of heterogeneities: study of the normalized Born ratio.* IEEE Trans Med Imaging, 2005. **24**(10): p. 1377-86.